EXTENDING THE OPERATING TEMPERATURE, WAVELENGTH AND FREQUENCY RESPONSE OF HgCdTe HETERODYNE DETECTORS*

D. L. Spears
Lincoln Laboratory, Massachusetts Institute of Technology
Lexington, Massachusetts 02173

ABSTRACT

Near-ideal optical heterodyne performance has been obtained at GHz IF frequencies in the 10-μm-wavelength region with liquid-nitrogen-cooled HgCdTe photodiodes. Heterodyne NEP's as low as 2.7×10^{-20} W/Hz at 100 MHz, 5.4×10^{-20} W/Hz at 1.5 GHz, and 9.4×19^{-20} W/Hz at 3 GHz have been achieved. Various physical phenomena which occur within a photodiode and affect heterodyne operation have been examined in order to assess the feasibility of extending the operating temperature, wavelength, and frequency response of these HgCdTe photomixers. Hole transit time is seen to limit the fundamental bandwidth of 10-μm HgCdTe photodiodes to about 5 GHz. Long optical absorption lengths and small depletion widths of 30-μm photodiodes lead to a response limited by minority electron diffusion. High dark current, very small depletion widths, and slow ambipolar diffusion affect the sensitivity and speed of high-temperature 10-μm HgCdTe photodiodes. For $T \gtrsim 200$ K, p-type HgCdTe photoconductors should outperform photodiodes as moderately-wide-bandwidth photomixers.

INTRODUCTION

In recent years the liquid-nitrogen-cooled HgCdTe photodiode has emerged as the superior wide-bandwidth infrared heterodyne detector in the 10-μm-wavelength region (refs. 1 and 2). High dc quantum efficiencies (75% to 90%) and RC roll-off frequencies in excess of 2 GHz have been routinely achieved (ref. 3). These devices have been used as photomixers at IF frequencies as high as 60 GHz (ref. 2). Quadrantal arrays (ref. 4) have been used in a monopulse CO_2 radar system (ref. 5) for the past five years, tracking at IF frequencies over 1.25 GHz at distances of over 1000 km. The field of laser heterodyne radiometry has made extensive use of these high-sensitivity HgCdTe photomixers for such applications as profiling gas distributions and wind velocities on planets (refs. 6 and 7), measuring ozone (ref. 8) and chlorine monoxide (ref. 9) concentrations in the earth's stratosphere, and stellar heterodyne interferometry (ref. 10).

In this paper, the state-of-the-art performance of HgCdTe photodiode heterodyne receivers and the physics associated with their operation will be discussed. Optical absorption coefficient, intrinsic carrier concentration,

*This work was sponsored by the National Aeronautics and Space Administration, the Defense Advanced Research Projects Agency, and the Department of the Air Force.

interband tunneling, minority-carrier diffusion, and hole transit time will be shown to present limitations and performance trade-offs for a HgCdTe photodiode heterodyne receiver operating at a frequency of 10 GHz, a wavelength of 30 μm, or a temperature near 200K. A discussion of p-type HgCdTe photoconductors for use as elevated-temperature CO_2-laser photomixers is also presented.

STATE OF THE ART

During the past ten years, high-performance HgCdTe photodiodes and photodiode arrays have been developed at Lincoln Laboratory (ref. 3) for use as wide-bandwidth heterodyne receivers. Numerous test measurements were also developed to evaluate these photodiodes and characterize their sensitivity and bandwidth in the heterodyne mode of operation. The blackbody heterodyne measurement has proven to be the most direct and reliable method for determining the heterodyne NEP at high frequencies. Here the measured signal-to-noise ratio is compared with that calculated for an ideal photomixer in order to obtain an effective heterodyne quantum efficiency η_{EH} (refs. 11 and 12) from which the NEP can be determined using the expression NEP = $h\nu B/\eta_{EH}$, where B (noise bandwidth) is usually normalized to 1 Hz. In figure 1 are shown the best values of NEP obtained to date (ref. 3) as a function of IF frequency from 10 MHz to 4 GHz. At 1 GHz the NEP is only about a factor of 2 above the quantum limit of an ideal photodiode-receiver system. A sensitivity of 6.2×10^{-20} W/Hz has also been reported (ref. 13) at 2 GHz. As the IF frequency increases, RC roll-off, diffusion effects, and higher preamplifier noise figures all contribute to a degradation in NEP of present HgCdTe photomixers. (The noise figures of the decade-bandwidth preamplifiers used to obtain the data in figure 1 ranged from about 1.1 dB at 10 MHz to 4.5 dB at 4 GHz.) The best results currently are below 1.5 GHz where most of the effort has been concentrated. Twelve-element arrays with <u>average</u> sensitivities of 7.1×10^{-20} W/Hz at 1.5 GHz and 4.3×10^{-20} W/Hz at 0.76 GHz have been demonstrated (refs. 3 and 14).

The values of NEP in figure 1 were obtained under optimum conditions of bias V_a (typically 0.3 to 0.7 volts) and LO power P_{LO} (typically 0.2 to 0.5 mW). In figure 2 is shown the NEP of a typical high-performance diode as a function of photocurrent ($I_{PC} = \eta(o) q P_{LO}/h\nu$, where $\eta(o)$ is the dc quantum efficiency) at 0.76 GHz and 1.5 GHz. The solid curves were calculated from the simple asymptotic expression (ref. 15) for NEP shown in figure 2, containing the ratios of preamplifier noise to shot noise and dark-current noise to shot noise. T_a is the effective noise temperature of the photodiode and preamplifier, and R_L is the effective load resistance. For a 10.6-μm photodiode at 77K, the dark-current term is almost always negligible at wide bandwidths. (Not all sources of dark current are noisy at high frequencies.) These calculated curves provide a good fit to the data up to $I_{PC} = 1$ mA. Beyond that, the NEP saturates at a value higher than given by the simple expression. In some photodiodes, the NEP <u>increases</u> with increasing photocurrent. This saturation is a result of physical changes within the photodiode caused by the intense optical flux $\phi \approx 1 \times 10^{20}$ photons/cm^2-sec. These processes are complicated, are not well understood, and vary considerably with detector geometry, impurity doping levels, and energy gap ε_g. Bandfilling, increased recombination, ambipolar effects, increased tunneling current, and simple heating can all contribute. These will be described in more

detail below. The effects are more important at high frequencies where larger values of photocurrent are required to overcome higher amplifier noise. By simple narrow-band impedance matching, we have been able to reduce the LO power requirement at 0.76 GHz from 150 μW (1 mA) as shown in figure 2 to about 50 μW (0.3 mA). This is very difficult to do for multioctave bandwidths, however.

PHOTODIODE PHYSICS

Basic Device Operation

Several effects can contribute to the response of a p-n junction photodiode: RC roll-off, the transit time of electrons and holes across the depletion region, the diffusion of holes from the n-type region to the space-charge region, and the diffusion of electrons from the p-type region to the space-charge region. The diffusion time can be as long as the lifetime of the minority carriers, which for 0.1-eV HgCdTe can be several microseconds (ref. 16). Obviously, such slow diffusion effects must be minimized for high-performance wide-bandwidth operation. The most successful wide-bandwidth HgCdTe detector structure to date has been the shallow-junction n^+n^-p geometry (ref. 4), a cross section of which is shown in figure 3. Here the junction depth is about 3 μm, and under reverse bias the depletion width is about 2 μm, leaving a 1-μm region of undepleted n-type material at the surface. Also shown in figure 3 is the expected absorption profile for 10.6-μm radiation, where the absorption coefficient α is about 3000 cm^{-1} (ref. 17).

Electron-hole pairs are created in all three regions, giving rise to several different response mechanisms. Holes produced in the n-type region must diffuse to the edge of the space-charge region and drift across in order to generate current. This diffusion time is approximately equal to $(\delta x)^2/D$, where δx is the distance from the space-charge layer where the electron-hole pair is produced and $D = \mu kT/q$ is the minority-carrier diffusion coefficient (ref. 18). Hole diffusion is a slow process as $D_h^{-1} \approx 2$ nsec/$(\mu m)^2$ at 77K, and only those holes produced within a fraction of a μm of the space-charge region will respond in 0.3 nsec (i.e., 1 GHz bandwidth). The diffusion length of holes (i.e., the average distance they can diffuse before they recombine) can be as long as 10 μm, so $\eta(o)$ could be very high for a junction as deep as 10 μm. However, such a device would have a very slow response, even though the junction capacitance may be small. For electron concentrations greater than about 10^{16} cm^{-3} the conduction band becomes degenerate and this band filling reduces the absorption near the cutoff wavelength in the n^+ layer and improves the high frequency performance (refs. 1 and 17).

The transit time across the depletion region is given by

$$t_t = \int_{w_D - x'}^{w_D} v(x')^{-1}\, dx' \qquad (1)$$

where w_D is the depletion width, x' is the position within the depletion region, and $v(x')$ is the local carrier drift velocity in the depletion region. At very low

fields, electrons in HgCdTe reach a scattering-limited saturation velocity due to their high mobility (ref. 16) and, consequently, travel across the space-charge region with constant velocity of about 2×10^7 cm/sec or $v_e^{-1} = 0.005$ nsec/μm. If electron transit were the only limitation, a 10-GHz bandwidth could be obtained with depletion widths as large as 6 μm. However, holes must also transit the space-charge region and they have a relatively small mobility ($\mu_h = 600$ cm^2/V-sec at 77K) and their drift velocity v_h is a function of position. For a 0.1-eV photodiode, v_h^{-1} is expected to vary from 0.02 nsec/μm to 2 nsec/μm.

Carriers generated in the p-type region are controlled by electron diffusion which can be relatively fast. Assuming $\mu_e = 30\ 000$ cm^2/V-sec in the p-type region, we obtain $D_e^{-1} = 0.05$ nsec/(μm)^2, which means that electron-hole pairs created in the p-type region within a few micrometers of the junction can respond at 1 GHz. However, if the minority-electron concentration approaches 1% of the hole density (by either thermal generation or the local-oscillator flux), ambipolar effects (ref. 19) enter and begin to slow this diffusion process.

The response of any given photodiode will be a composite of all the above effects and the RC roll-off due to the external circuit and the junction capacitance. The relative importance of each of these processes will depend on the precise junction depth, doping levels, HgCdTe alloy composition, and the local-oscillator flux level.

Slow diffusion, which can frequently be seen as a tail on the pulse response of a photodiode, is particularly detrimental to heterodyne operation. This diffusion not only gives rise to a loss in signal at high frequency, but gives additional noise, as the slowly diffusing carriers have the same shot-noise spectra as the fast ones (ref. 20). The shot-noise-limited NEP in the presence of diffusion is given by

$$\mathrm{NEP}_{\min} = \frac{h\nu B}{\eta(0)} \left[\frac{\eta(0)}{\eta(f)} \right]^2 \tag{2}$$

where $\eta(f)$ is the quantum efficiency at frequency f. In a planar diode, lateral diffusion from around the perimeter can degrade its high-frequency performance. To get maximum sensitivity, the local oscillator should be confined to within the junction area. A steep mesa diode does not have this lateral diffusion problem.

Optical-Absorption Coefficient

A high value of optical absorption coefficient α is desirable in a wide-bandwidth photodiode in order to localize the photocarrier generation. However, in small-energy-gap material, α is not very large. In figure 4 is shown the wavelength dependence of α as given by the Kane theory (ref. 17) for HgCdTe with energy gaps of 0.1 eV and 0.035 eV, required for 10.6-μm and 30-μm photodiodes, respectively. Accurate experimental values have been reported only for $\alpha < 1000$ cm^{-1}. However, these calculated curves are consistent with all published

data and with transmission measurements made at Lincoln Laboratory on thin epitaxial samples. The solid curves do not take into account effects of charge carriers, impurities, or lattice vibrations, all of which tend to "smear out" the absorption edge. Band filling occurs in narrow-energy-gap HgCdTe with relatively low electron concentrations due to the small density of states in the conduction band. This produces a Burstein-Moss shift in the absorption edge as indicated by the dashed curves in figure 4, which show the effects of 1×10^{16} electrons/cm^3 in 0.1-eV HgCdTe and 1×10^{15} electrons/cm^3 in 0.035-eV HgCdTe. These electron densities are similar to those optically generated by a 100-μm-diameter LO beam producing I_{PC} = 1 mA. Thus if the background doping does not render the n-type region transparent near the absorption edge, the LO flux most likely will. At a wavelength of 10 μm, the absorption length $1/\alpha$ is about 3 μm, whereas for λ = 30 μm, $1/\alpha$ is about 10 μm. Confinement of the photocarrier generation is particularly difficult at 30 μm.

Tunneling Breakdown

The fundamental breakdown mechanism in a reverse-biased, narrow-energy-gap photodiode is the tunneling of electrons from the valence band to the conduction band due to the high field in the space-charge region. In a one-sided abrupt junction this field varies linearly across the depletion layer with a peak value of $2V/w_D$, where V is the sum of the external bias and the built-in junction potential ($\sim \varepsilon_g/2q$). The depletion width is given by

$$w_D = (2\kappa V/qN)^{1/2} \qquad (3)$$

where κ is the dielectric constant (~18.6 for $Hg_{0.8}Cd_{0.2}Te$) and N is the carrier concentration on the lightly-doped side of the junction. The value of w_D at breakdown sets a limit to the RC roll-off frequency of the device. In figure 5 is shown the calculated depletion width at a tunnel-current density of 1 A/cm^2 as a function of N for energy gaps of 0.1 eV and 0.035 eV, according to equation 16 of reference 21. The peak field at breakdown E_{max} is a strong function of energy gap ($E_{max} \propto \varepsilon_g^{5/3}$) but is relatively independent of N. E_{max} at J_T = 1 A/cm^2 is about 1 V/μm for ε_g = 0.1 eV and 0.17 V/μm for ε_g = 0.035 eV. As can be seen in figure 5, w_D at breakdown is a strong function of N and ε_g, varying approximately as $\varepsilon_g^{1.43}/N^{0.9}$. For ε_g = 0.1 eV, depletion widths in excess of 6 μm should be obtainable with present HgCdTe material technology ($N \sim 1 \times 10^{14}$ cm^{-3}). In high-performance wide-bandwidth photodiodes, w_D has been typically in the range of 2 to 3 μm at breakdown. A 1-GHz RC roll-off frequency into 50 Ohms for a 100-μm-diameter photodiode requires $w_D > 0.4$ μm, which is achieveable with $N = 2 \times 10^{15}$ cm^{-3} in 0.1-eV material. Clearly very high RC roll-off frequencies are possible with carrier concentrations in the low 10^{14} cm^{-3} range. A device sensitive at a wavelength of 30 μm, however, requires N to be less than 3×10^{14} cm^{-3} for a 1-GHz RC roll-off.

Intrinsic Carrier Concentration

A high density of carriers can be generated thermally in small-energy-gap semiconductors. In figure 6 is shown this intrinsic carrier concentration n_i as a function of temperature for $\varepsilon_g = 0.1$ eV and $\varepsilon_g = 0.035$ eV (ref. 22). For good diode characteristic, n_i should be much less than the doping levels on either side of the junction. For a wide-bandwidth 30-μm photodiode, this requires operation below about 50K to achieve n_i less than 10^{14} cm^{-3}, as seen from figure 6. Similarly a 10-GHz 10.6-μm diode must be operated below about 100K. Note as the 0.1-eV material approaches 200K, n_i becomes greater than 10^{16} cm^{-3}. Thus from figure 5 we see that the depletion width at breakdown in a high-temperature 10.6-μm photodiode will be much less than 1 μm and, since $1/\alpha > 3$ μm, its response will be diffusion limited.

Photogenerated Carriers

The LO flux can cause enormous changes in the minority (and majority) electron and hole concentrations in a photodiode. In the absence of drift and diffusion effects, the steady-state excess photocarrier concentration is given simply by $\alpha \phi \tau$, where τ is the minority-carrier lifetime. In lightly doped 0.1-eV n-type HgCdTe, τ_h is of the order of 10^{-6} sec (ref. 16), so $\alpha \phi \tau_h \approx 3 \times 10^{17}$ cm^{-3} for $\phi = 10^{20}$ photons/cm^2-sec. This electron concentration would clearly give strong band filling (see figure 4) and render the material transparent near the absorption edge. Near a p-n junction, diffusion and drift effects must be considered, however (see reference 19). The excess minority-electron concentration δn in the p-type side of an n-p junction illuminated from the n-type side is given by

$$\delta n(x) = \alpha \phi \tau_e \quad (\exp(-x/L_e) - \exp(-\alpha x))/(\alpha^2 L_e^2 - 1) \qquad (4)$$

$$\alpha L_e \neq 1$$

where x is the distance from the space-charge region, and $L_e = (D_e \tau_e)^{1/2}$ is the minority-electron diffusion length. Figure 7 shows $\delta n(x)$ calculated using parameters appropriate for a typical 10.6-μm HgCdTe photodiode at moderate LO flux. The minority-electron lifetime τ_e is a strong function of hole concentration and 10 nsec is believed appropriate for a hole concentration p in the region of 3×10^{16} cm^{-3} at 77K (ref. 23). Note, the calculated photoelectron density peaks at a value of about 1×10^{14} cm^{-3} at a distance from the junction about equal to the absorption length. At this concentration, these minority electrons contribute significantly to the conductivity due to the high electron-to-hole mobility ratio b (~100 in HgCdTe). In this ambipolar regime (ref. 19), the diffusion coefficient is given by

$$D_a = D_e \, (1 + n/p)/(1 + b \, n/p) \qquad (5)$$

where $n = \delta n + n_0$. As n approaches p/b, D_a decreases, slowing down the diffusion process, which in turn reduces the frequency response and quantum

efficiency. For low values of p, ambipolar effects enter in at lower values of optical flux. In the very-strong-flux limit, the lifetime, the mobility, and the absorption coefficient are all expected to be functions of LO power, and a self-consistent calculation of $\delta n(x)$ is very difficult.

ULTRAWIDE-BANDWIDTH PHOTODIODES

With increasing bandwidth, hole transit time begins to affect the response of a 10-μm HgCdTe photodiode, as the hole velocity v_h within the space-charge region is low and a function of position, $v_h(x) = \mu_h E(x)$. In the case of a one-sided abrupt junction, $E(x)$ varies linearly across the space-charge region. If we assume $v_h(x) = (x/w_D)\, v_m + v_o$, then integrating equation 1 we obtain the transit time,

$$t_t(x) = \frac{w_D}{v_m} \ln \left\{ \frac{w_D}{x} \left(\frac{1 + v_o/v_m}{1 + (v_o/v_m)(w_D/x)} \right) \right\} \qquad (6)$$

for a hole generated within the space-charge region a distance x from the n-type side. Using this expression we have made numerous numerical calculations of the step response of photodiodes assuming: 1) the photogeneration varies exponentially into the device as $e^{-\alpha x}$ and 2) the delay in the response of each of these photogenerated carriers is given by the sum of their diffusion time $(\delta x)^2/D$ and transit time, i.e. the time required for holes to reach the p-type region and electrons to reach the n-type region. For $1/\alpha \ll w_D$ (which is the common situation for wide-energy-gap, high-speed photodiodes), a shallow-junction p^+-n^- device is the best structure for minimizing hole-transit effects as the electron-hole pairs are generated near the p^+ side of the depletion layer and only electron transit is involved. However, for small absorption coefficients, such as here at $\lambda \approx 10\mu m$, the difference between an n-p and p-n diode structure is small. The step response calculated for two n^+n^-p photodiodes with depletion widths of 4 μm are shown in figure 8. Here the RC time constant is assumed zero and the undepleted n^+-region is assumed transparent, i.e. no hole-diffusion effects. The curve on the right is for a simple triangular field profile (E_{max} = 1 V/μm). Electrons generated near the p side of the space-charge region give the initial response after a 15-psec transit time delay. The slower rise continuing to about 120 psec is the delayed response of holes produced throughout the space-charge region. If the thickness of the n^- region is only 4 μm and very lightly doped (i.e. pin-type device), "punch through" can occur well before breakdown, giving a more uniform field profile as shown in the diagram on the left in figure 8. If the average field is 75% of the breakdown field (i.e. 0.75 V/μm), the step response on the left is calculated. The very slow rise at the top is due to the comparatively slow diffusion of photoelectrons produced in the p-type region. Transit time could be reduced by decreasing the width of the space-charge layer; however, this would result in a loss in quantum efficiency and increased junction capacitance. We chose w_D = 4 μm here because it is greater than $1/\alpha$ and gives a 10-GHz RC roll-off frequency for a 100-μm-diameter photodiode. Judging from the step response shown in figure 8, a 10-GHz bandwidth (which requires a 30-psec rise time) does

not appear possible in a 10.6-μm HgCdTe photodiode. The fundamental bandwidth limit will be about 5 GHz. However, since the shot noise spectra is also influenced by transit time (ref. 24) (both the signal and the shot noise will roll off between 5 and 10 GHz), reasonably good sensitivity (1×10^{-19} W/Hz) may be possible at 10 GHz in an optimized device.

LONG-WAVELENGTH PHOTODIODES

In figure 9 is shown the reverse-bias I-V characteristic calculated for a 100-μm-diameter, 0.035-eV n^--p photodiode at 40K with $n^- = 2 \times 10^{14}$ cm^{-3}. For the case of Auger-limited lifetimes (refs. 16 and 23) used here, the dominant diffusion component is from the p-type side and given by

$$I_D = A\,(n_i^2/p)\,e(D_e/L_e) \qquad (7)$$

where A is the photodiode area. As seen from figure 9, this current is small ($\sim$0.1 A/cm^2) at 40K. The tunnel current I_T shows a characteristic soft breakdown. The magnitude of I_T is not a problem for V < 100 mV; however, for the impedance dV/dI to be greater than 50 Ohms, the bias must be below about 60 mV, where $w_D = 0.7$ μm. Since $1/\alpha \gtrsim 10$ μm, essentially all of the photocarrier generation takes place in the p-type region. In a thick photodiode, the frequency response limited by electron diffusion is approximately $\alpha^2 D_e$ (ref. 24), which for T = 40K, μ_e = 50 000 cm^2/V-sec and α = 1000 cm^{-1}, is about 250 MHz. A diffusion-limited bandwidth of 1 GHz could be obtained by thinning the p-type region to about 3 μm. With a reflecting contact to increase the absorption, a quantum efficiency of 40% should be possible. However, a very important question remains. The minority electron mobility μ_e is expected to be a function of hole concentration. Can μ_e = 50 000 cm^2/V-sec be obtained with $p = 1 \times 10^{16}$ cm^{-3} in 0.035-eV HgCdTe ? A concentration much less than this will be susceptible to strong ambipolar effects. If these parameters are consistent, then an NEP of about 5×10^{-20} W/Hz at 1 GHz should be possible at 30 μm.

ELEVATED-TEMPERATURE PHOTODIODES

There has been great interest in developing CO_2 laser photomixers operating at temperatures in the region of 200K where thermoelectric coolers are convenient, reliable and reasonably efficient. At elevated temperatures, narrow-energy-gap photodiodes are subject to very high dark current in reverse bias due to diffusion, drift and/or tunneling. If the minority-carrier recombination times in a 0.1-eV photodiode are Auger-limited (refs. 16 and 23), then electron-diffusion current from the p-side of the junction is the dominant diffusion component and relatively independent of p. In the Auger limit, τ_e varies as $1/p^2$ (see reference 23). In figure 10 is shown this diffusion current (calculated from equation 7) as a function of temperature for energy gaps of 0.11 eV and 0.14 eV, corresponding to α = 1000 cm^{-1} at 11 μm and 9 μm (ref. 25), respectively. Also shown are data taken on a photodiode with a cutoff wavelength of about 9 μm at 185K, which are in reasonable agreement with these calculations. Diffusion current can be reduced by thinning the p-type region in order to limit the diffusion volume (ref. 19). However, diffusion-current

values below these curves in figure 10 are yet to be reported. Also, this simple theory is not strictly valid at these very high current densities ($\sim$100 A/cm^2). If either n or p is close to the value of n_i, a large component of drift current also flows across the junction; whereas if n and p are both much greater than n_i, tunneling current becomes excessive at even very low biases. In both of these cases, the calculated maximum reverse-bias resistance of a 200K 0.12-eV HgCdTe photodiode is only a few ohms. The frequency response at high temperatures of an optimally designed shallow-junction n-p photodiode is determined by minority-electron diffusion, which is in the strong ambipolar regime. Here, as seen from equation 5, D_a approaches 2 D_e/b and the absorption-limited diffusion time increases into the range of 10 to 50 nsec. Faster response can be achieved by heavily doping the p-type region and reducing the lifetime of the minority electrons, but this is at the expense of quantum efficiency.

At 173K, we have measured an NEP of 4 x 10^{-19} W/Hz at 9.3 μm for a 90-MHz photodiode, and an NEP of 8 x 10^{-19} W/Hz at 10.6 μm has been reported (ref. 26) also at 173K for a 23-MHz device. With further development, NEPs approaching 1 x 10^{-19} W/Hz and bandwidths approaching 100 MHz should be realized in 180K photodiodes. This performance will be very sensitive to temperature, however.

p-TYPE HgCdTe PHOTOCONDUCTORS

As the performance of HgCdTe photodiodes degrades with increasing temperatures, the p-type HgCdTe photoconductor becomes very attractive as a moderately-wide-bandwidth CO_2-laser photomixer. In this device, the bandwidth and photoresponse are determined by the lifetime τ_e and mobility μ_e of the minority electrons. In addition, the resistance can be reasonably high at 200K due to the low mobility of holes. In order to obtain quantum-noise-limited performance in a p-type photoconductor (NEP = 2 $h\nu B/\eta$), the LO power must be such that (1) the density of photoelectrons greatly exceeds the background minority electron density (n_i^2/p) and (2) the associated g-r noise greatly exceeds the Johnson or thermal noise 4kT/R of the detector and preamplifier (ref. 24). Both of these requirements are very sensitive to n_i, μ_e, and τ_e. The dashed curve in figure 11 shows the photoconductor bandwidth $(2\pi\tau_e)^{-1}$ determined from the calculated Auger-limited lifetime (ref. 23) as a function of hole concentration at 200K for 0.12-eV HgCdTe (n_i = 1 x 10^{16} cm^{-3}). Using this theoretical lifetime and assuming μ_e = 10 000 cm^2/V-sec, we have calculated (unpublished work of D. L. Spears, P. E. Duffy, and C. D. Hoyt) the LO power required in order to achieve a photoelectron concentration equal to the background electron concentration and a g-r noise equal to the thermal noise. These values of P_{LO} are a strong function of p as shown by the solid curves in figure 11. A minimum in the calculated LO power occurs for p = 3 x 10^{16} cm^{-3}, with a corresponding bandwidth of 12 MHz. Note, for a 100 MHz bandwidth, the calculated CO_2 LO power is about 10 mW. The over-100-mW requirement at 1 GHz is unreasonable, as excessive heating (ΔT > 100K) would surely occur in these small-area (100 μm x 100 μm) devices.

P-type photoconductors we have fabricated have shown a 9.3-μm NEP of about 2 x 10^{-19} W/Hz at 38 MHz at 200K, with a bandwidth of over 50 MHz and a LO power requirement of 7 mW. Other devices with bandwidths in excess of

150 MHz have shown NEPs better than 4×10^{-19} W/Hz at 200K. With the optimum geometry, energy gap, and hole concentration, we expect that an NEP of about 1×10^{-19} W/Hz at 100 MHz could be achieved in a 200K photoconductor with a total power dissipation of 10 mW, which is compatible with a 1-watt TE cooler.

REFERENCES

1. C. Verie and M. Sirieix "Gigahertz Cutoff Frequency Capabilities of CdHgTe Photovoltaic Detectors at 10.6 μm," IEEE J. Quantum Electron., vol. QE-8, pp. 180-191, Feb. 1972.

2. D. L. Spears and C. Freed "HgCdTe Varactor Photodiode Detection of cw CO_2 Laser Beats Beyond 60 GHz." Appl. Phys. Lett., vol. 23, pp. 445-447, Oct. 1973.

3. Solid State Research Reports, Lincoln Laboratory, M.I.T. (1970:4), (1973:2), (1974:4), (1975:3), (1976:3), (1977:1), (1977:4), (1978:1) and (1978:3).

4. D. L. Spears "Planar HgCdTe Quadrantal Heterodyne Arrays with GHz Response at 10.6 μm," Infrared Phys., vol. 17, pp. 5-8, Jan. 1977.

5. R. Teoste, W. J. Scouler and D. L. Spears "Coherent Monopulse Tracking with a 10.6-μm Radar," Digest of Technical Papers, 1977 IEEE/OSA Conf. on Laser Engineering and Applications, pp. 40-41, June 1-3, 1977, Washington, D.C. (IEEE, New York, 1977).

6. A. L. Betz, R. A. McLaren, E. C. Sutton and M. A. Johnson "Infrared Heterodyne Spectroscopy of CO_2 in the Atmosphere of Mars," Icarus, vol. 30, pp. 650-662, 1977.

7. T. Kostiuk, M. J. Mumma, J. J. Hillman, D. Buhl, L. W. Brown, J. L. Faris and D. L. Spears "NH_3 Spectral Line Measurements on Earth and Jupiter using a 10-μm Superheterodyne Receiver," Infrared Phys., vol. 17, p. 431-439, Nov. 1977.

8. M. A. Frerking and D. J. Muehlner "Infrared Heterodyne Spectroscopy of Atmospheric Ozone," Appl. Optics, vol. 16, pp. 526-528, Mar. 1977.

9. R. T. Menzies "Remote Measurement of ClO in the Stratosphere," Geophys. Res. Lett., vol. 6, p. 151-154, Mar. 1979.

10. E. C. Sutton, J. W. V. Storey, A. L. Betz, C. H. Townes and D. L. Spears "Spatial Heterodyne Interferometry of VY Canis Majoris, Alpha Orionis, Alpha Scorpii, and R Leonis at 11 Microns," Astrophys. J. (Letters), vol. 217, pp. L97-L100, Oct. 1977.

11. B. J. Peyton, A. J. DiNardo, S. C. Cohen, J. H. McElroy and R. J. Coates "An Infrared Heterodyne Radiometer for High-Resolution Measurements of Solar Radiation and Atmospheric Transmission," IEEE J. Quantum Electron., vol. QE-11, pp. 569-574, Aug. 1975.

12. R. T. Ku and D. L. Spears "High-Sensitivity Infrared Heterodyne Radiometer Using a Tunable-Diode-Laser Local Oscillator," Optics Lett., vol. 1, pp. 84-86, Sept. 1977.

13. J. F. Shanley and L. C. Perry "Wide Bandwidth 10.6 μm (Hg,Cd)Te Photodiodes for Infrared Heterodyne Applications," Tech. Digest of the Int. Electron Device Meeting, pp. 424-429, Dec. 1978, Washington, D.C.

14. D. L. Spears "Wide Bandwidth CO_2 Laser Photomixers," Proc. of the S.P.I.E., vol. 227, 1980.

15. B. J. Peyton, A. J. DiNardo, G. M. Kanischak, F. R. Arams, R. A. Lang and E. W. Sard "High-Sensitivity Receiver for Infrared Laser Communications," IEEE J. Quantum Electron., vol. QE-8, pp. 252-263, Feb. 1972.

16. R. Dornhous and G. Nimtz "The Properties and Applications of the $Hg_{1-x}Cd_xTe$ Alloy System," in Solid State Physics 78, G. Hohler, ed. (Springer-Verlag, New York, 1966).

17. M. D. Blue "Optical Absorption in HgTe and HgCdTe," Phys. Rev., vol. 134, p. A226-A234, Apr. 1964.

18. D. E. Sawyer and R. H. Rediker, "Narrow Base Germanium Photodetectors," Proc. IRE, vol. 46, pp. 1122-1130, June 1958.

19. John P. McKelvey, Solid State and Semiconductor Physics (Harper and Row, New York, 1966).

20. D. L. Spears and R. H. Kingston "Anomalous Noise Behavior in Wide Bandwidth Photodiodes in Heterodyne and Background-Limited Operation," Appl. Phys. Lett., vol. 34, pp. 589-590, May 1979.

21. W. W. Anderson "Tunnel Current Limitations of Narrow Bandgap Infrared Charge Coupled Devices," Infrared Phys., vol. 17, pp. 147-164, Mar. 1977.

22. Y. Nemirovsky and E. Finkman "Intrinsic Carrier Concentration of $Hg_{1-x}Cd_xTe$," J. Appl. Phys., vol. 50, pp. 8107-8111, Dec. 1979.

23. T. N. Casselman and P. E. Peterson "A Comparison of the Dominant Auger Transitions in p-type (Hg,Cd)Te," Solid State Comm., vol. 33, pp. 615-619, Feb. 1980.

24. R. H. Kingston, Detection of Optical and Infrared Radiation, (Springer-Verlag, New York, 1978).

25. E. Finkman and Y. Nemirovsky "Infrared Optical Absorption of $Hg_{1-x}Cd_xTe$," J. Appl. Phys., vol. 50, pp. 4356-4361, June 1979.

26. T. Koehler "10.6 Micron (Hg,Cd)Te Photodiode Module," Research and Development Report, Honeywell Radiation Center, ECOM-71-0236-F, Oct. 1976.

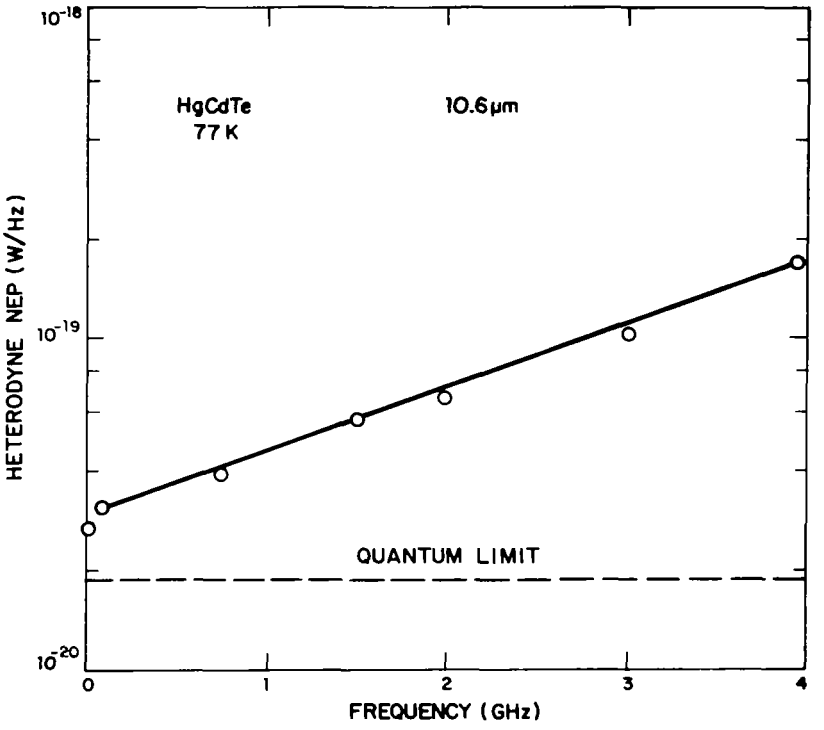

Figure 1.- State-of-the-art heterodyne NEP at 10.6 μm as function of IF frequency.

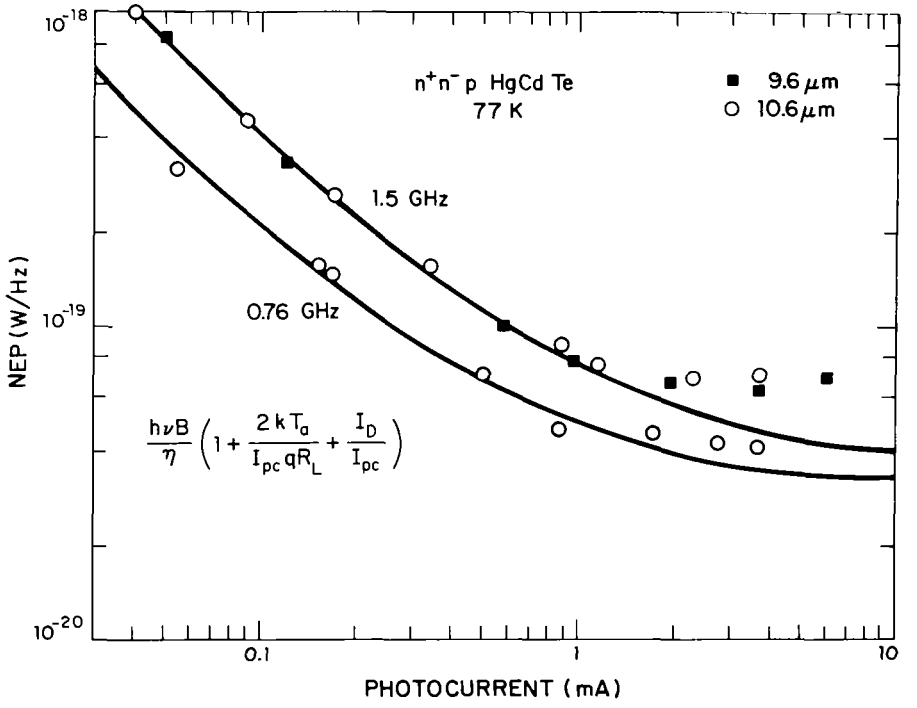

Figure 2.- Heterodyne NEP as function of LO-induced photocurrent for high-performance HgCdTe photodiode.

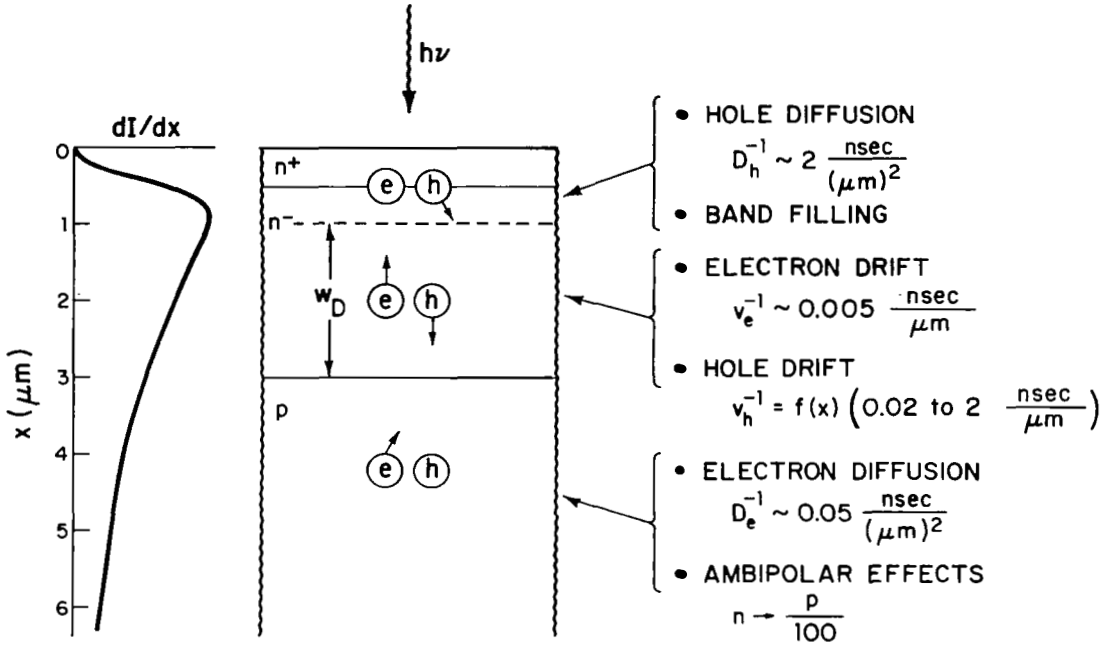

Figure 3.- Cross section of n^+n^-p HgCdTe photodiode showing absorption profile at 10.6 μm and drift and diffusion parameters at 77 K.

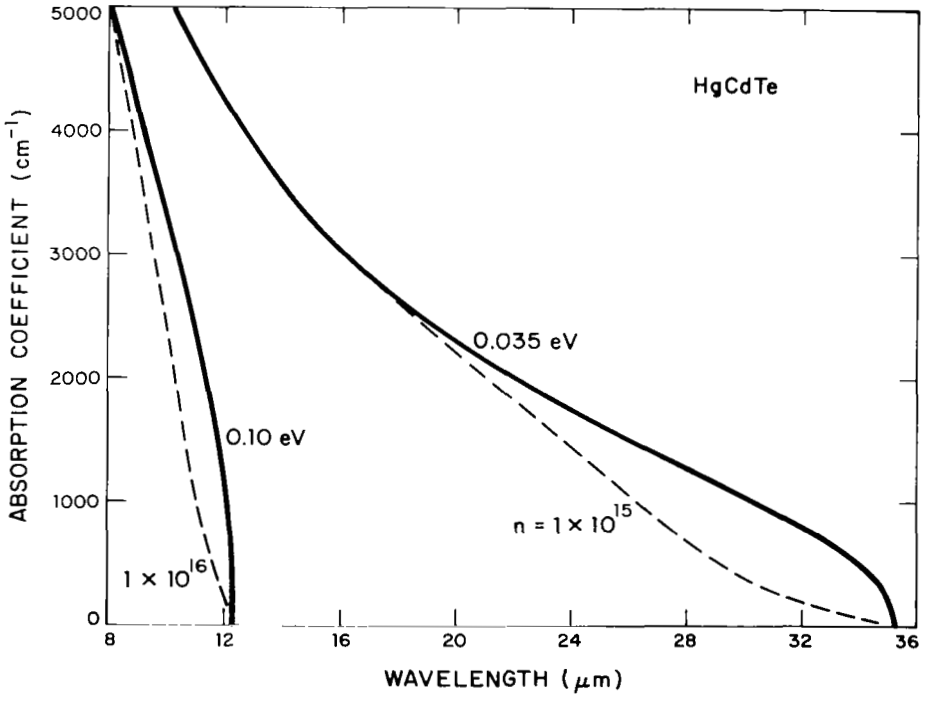

Figure 4.- Calculated optical absorption coefficient as function of wavelength for HgCdTe with energy gaps of 0.1 and 0.035 eV.

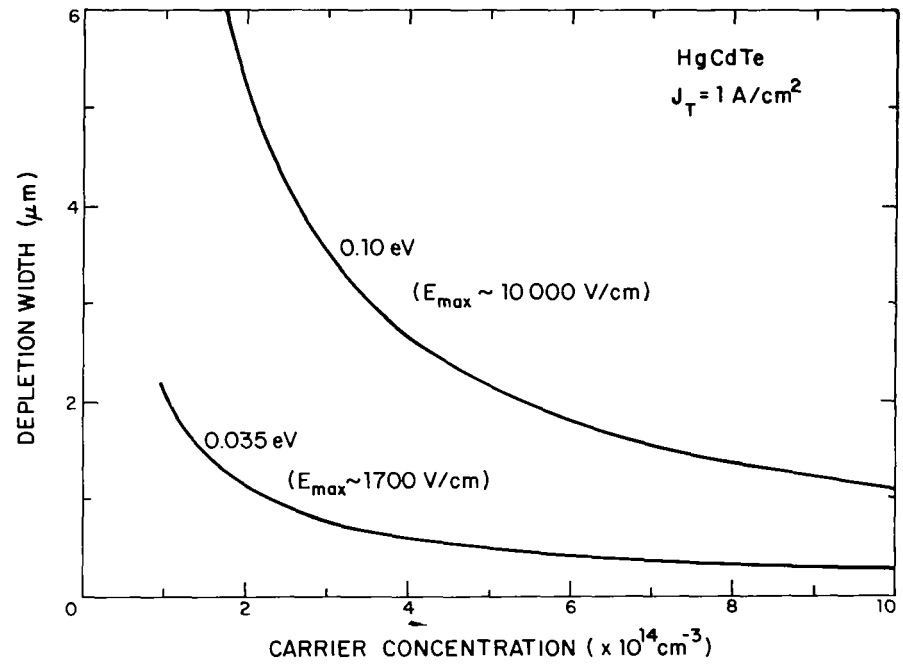

Figure 5.- Calculated junction depletion width at tunnel current density of 1 A/cm^2 as function of carrier concentration for one-sided abrupt junctions in HgCdTe with energy gaps of 0.1 and 0.035 eV.

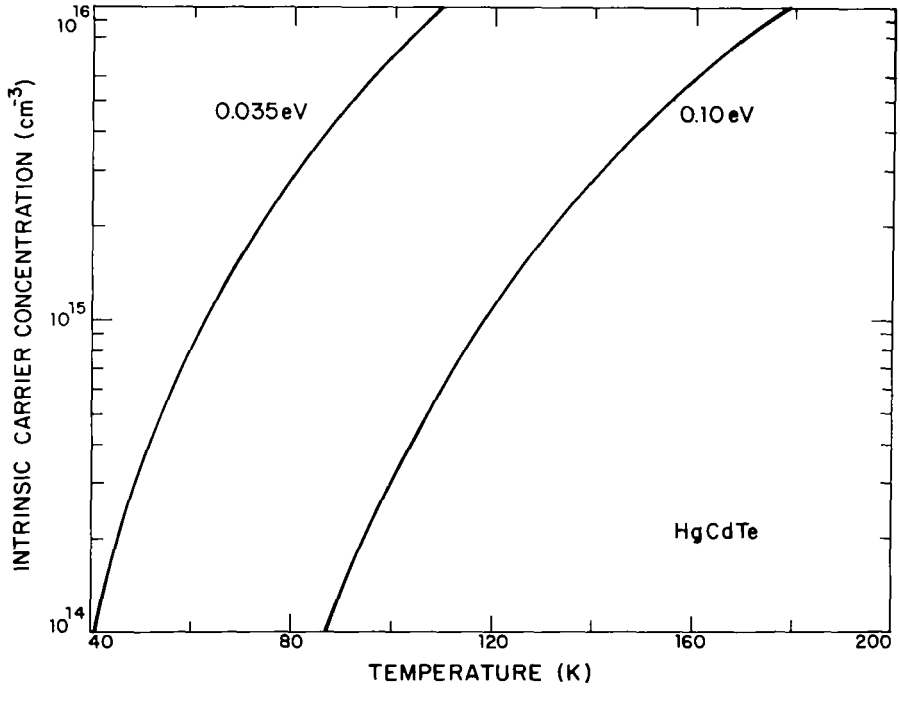

Figure 6.- Intrinsic carrier concentration as function of temperature for HgCdTe with energy gaps of 0.1 and 0.035 eV (ref. 22).

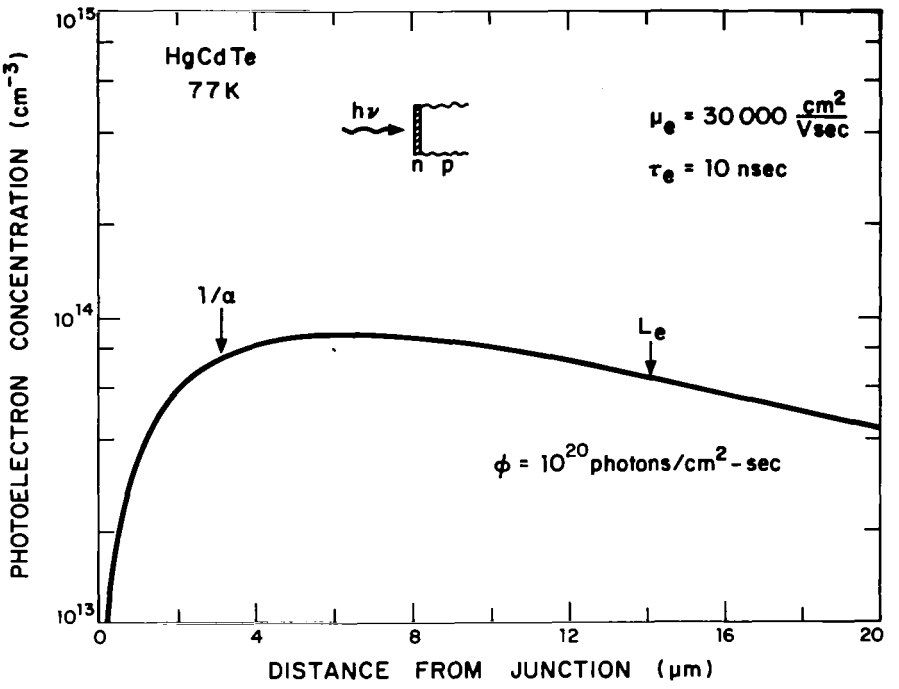

Figure 7.- Calculated steady-state minority electron distribution in n-p HgCdTe photodiode for typical LO flux level.

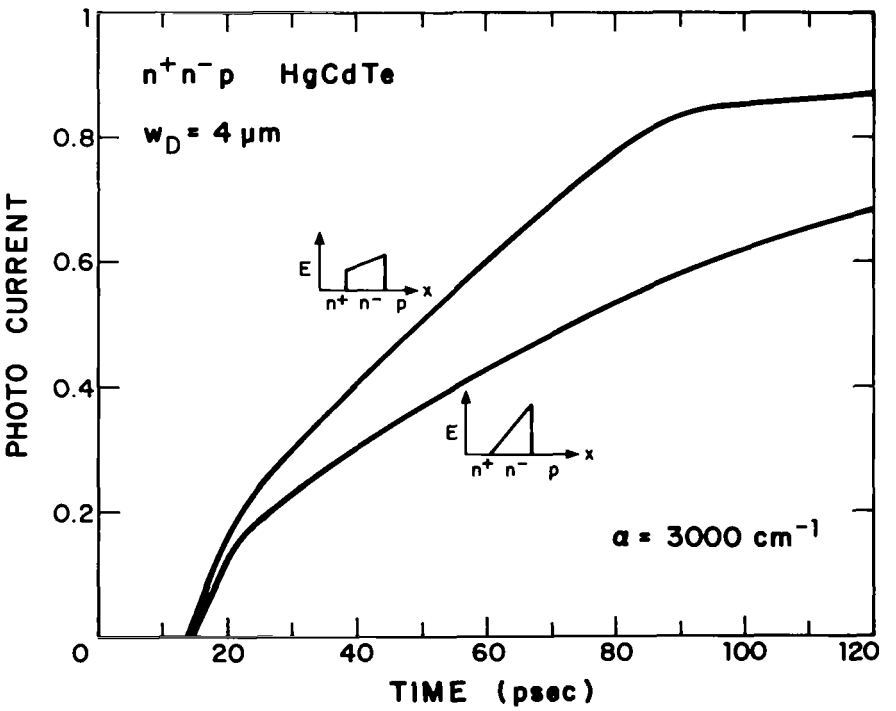

Figure 8.- Calculated step response of two reverse-biased n^+n^-p HgCdTe photodiodes (assuming RC = 0) showing transit time delays.

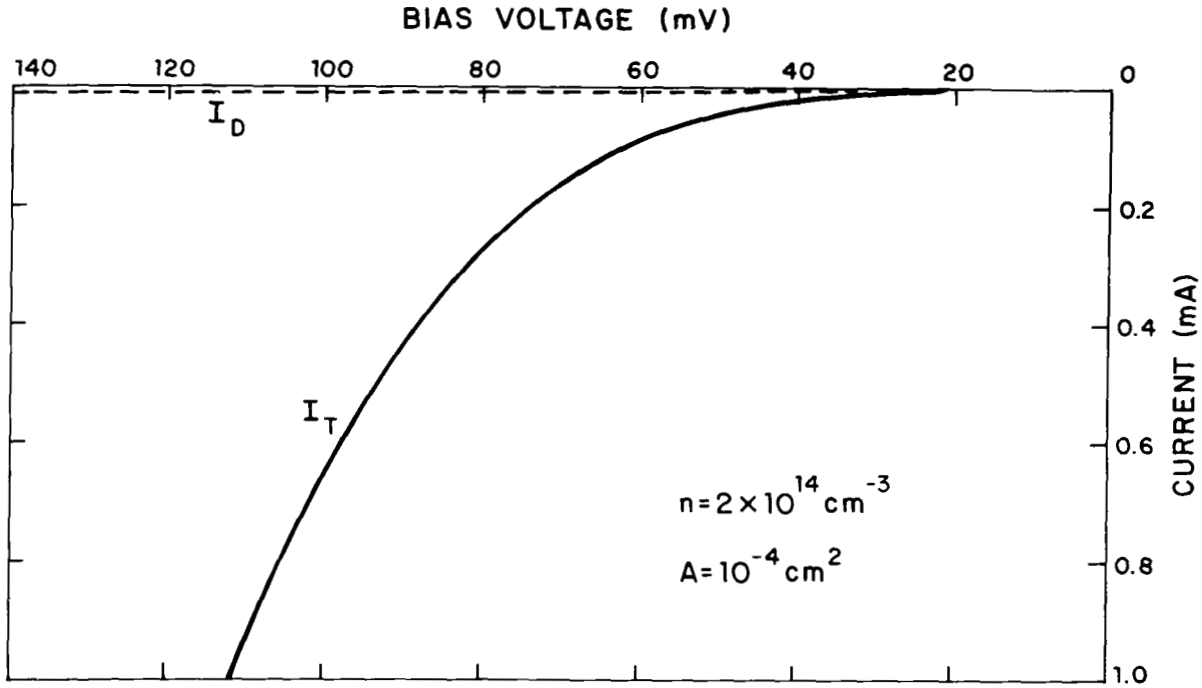

Figure 9.- Calculated reverse-bias I-V characteristic for 30-μm HgCdTe photodiode at 40 K.

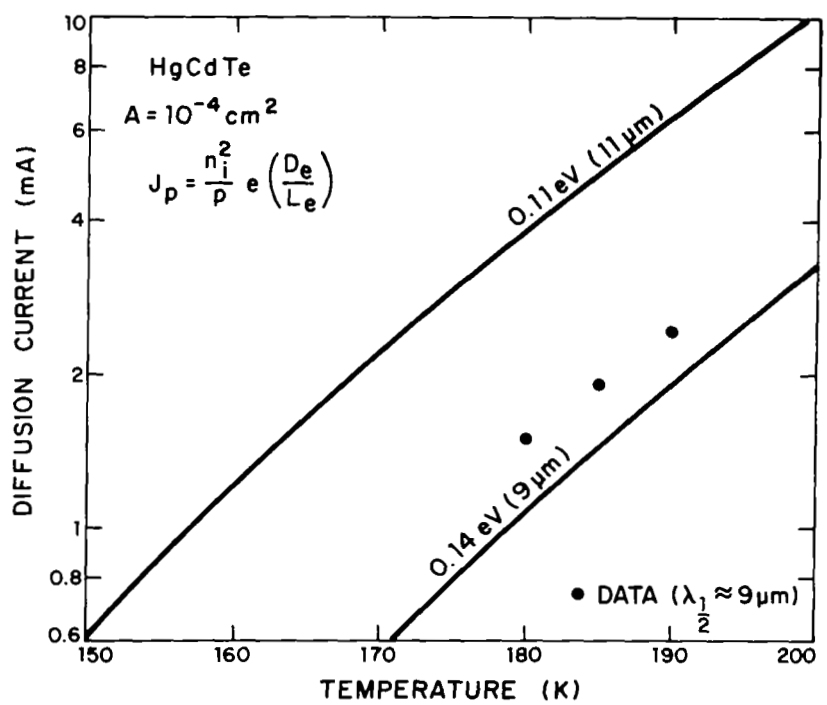

Figure 10.- Calculated diffusion current as function of temperature for HgCdTe photodiodes with energy gaps of 0.11 and 0.14 eV, along with data for 9-μm photodiode.

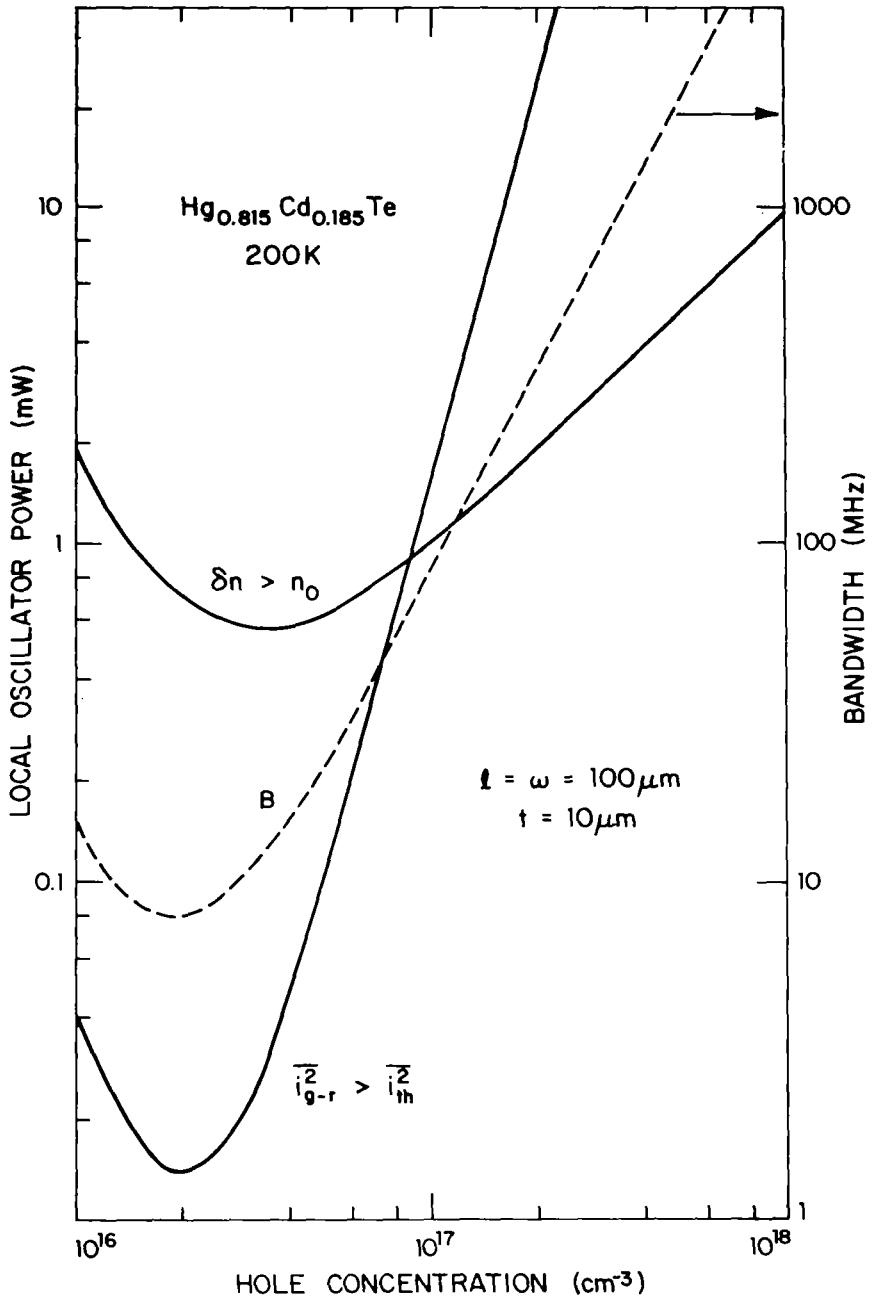

Figure 11.- Calculated bandwidth and heterodyne LO power requirements at 200 K as function of hole concentration for p-type HgCdTe photoconductors.